

# Results from BRAHMS experiment at RHIC

Eun-Joo Kim<sup>a</sup> for the BRAHMS Collaboration

<sup>a</sup>Institute of Proton Accelerator, Chonbuk National University, Jeonju, 561-756, Korea

We review briefly recent results obtained by BRAHMS Collaboration at Relativistic Heavy Ion Collider. The rapidity and centrality dependence of charged particle production in Au+Au, Cu+Cu, and p+p at energies  $\sqrt{s_{NN}} = 200$  and 62.4 GeV is presented. Studying of nuclear modification factor, elliptic flow and coalescence parameter as a function of rapidity gives an additional constraints on mechanisms describing dynamics of hadronic/partonic matter created in high energy heavy ion collisions.

## 1. Introduction

The main purpose of studying heavy ion collisions at relativistic energy is to understand the matter characterized by a large density of deconfined quarks and gluons (QGP) [1,2]. Hadron with high transverse momentum provide a good information of the high energy density matter produced in relativistic heavy ion collisions, since the production of high  $p_T$  particle is a result of strong hard parton-parton scatterings with large momentum transfer. After hard-scattering, partons traverse a medium with a high density of color charges where they interact strongly, emit gluon radiation, and lose energy before fragmenting into hadrons. The production of hadrons depends on the initial parton distributions in the colliding nuclei, the elementary parton-parton cross section and the hadronization process of partons into hadrons. In order to fully understand these phenomena, it is important to study the hadron production in a wide kinematic range.

The BRAHMS experiment [3,4] has studied rapidity dependence of particle production from  $y = 0$  to  $y = 3.5$  for Au+Au, Cu+Cu, and p+p collisions at  $\sqrt{s_{NN}} = 200$  and 62.4 GeV. The data were obtained with two movable BRAHMS magnetic spectrometer arms, and global detector systems for event characterization and determination of interaction point. By rotating the arms within the small and large particle emission angles, BRAHMS is able to study the properties of the produced medium as a function of its longitudinal expansion. The collision region is surrounded by arrays of silicon and scintillating tile detectors [5]. Three azimuthally symmetric rings of Si detectors and one ring of tile detectors are used in the reaction-plane analysis. For p+p collisions additional Čerenkov radiators are used to determine the interaction vertex with a resolution of  $\sim 2$ cm.

## 2. Results

High  $p_T$  suppressions have been observed in central Au+Au collisions at RHIC [6–8] and are attributed to final-state interactions based on the absence of such suppressions

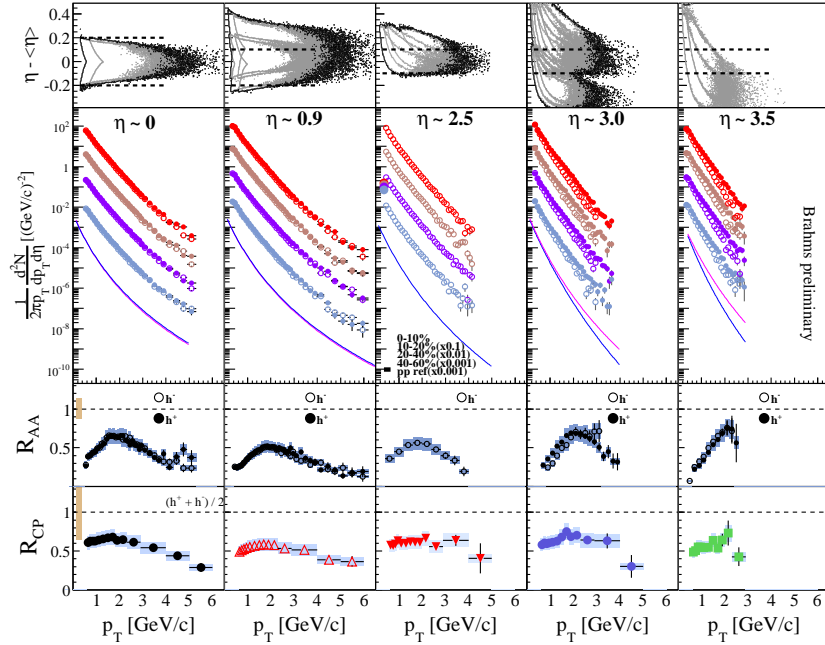


Figure 1. Population of data in  $\eta - \langle \eta \rangle$  vs.  $p_T$  for each setting is shown in top panel. The middle panels show charged hadron spectra for several centralities in Au+Au collisions at  $\sqrt{s_{NN}} = 200$  GeV at  $\eta = 0, 1.0, 2.5, 3.0$  and  $3.5$ . The full drawn lines are fits to the measured p+p spectra. The bottom panels show the nuclear modification factor  $R_{AA}$  and  $R_{CP}$  at different  $\eta$  for the most central collisions. The shaded bar at 1 shows the error on the scale.

in d+Au collisions [9–12]. The suppression is quantified by use of nuclear modification factors, which are defined as  $R_{AA}$  or  $R_{CP}$ .  $R_{AA}$  gives the deviation in yields from AA collisions relative to the scaled yields from nucleon-nucleon collisions.  $R_{CP}$  can provide similar information based on the relative yield in central(C) and peripheral(P) collisions scaled by the mean number of binary collisions, but does not depend on the reference nucleon-nucleon system. Figure 1 shows the charged hadrons spectra from Au+Au collisions at  $\sqrt{s_{NN}} = 200$  GeV for several centrality bins and at different pseudorapidities. Each distribution is constructed from measurements at the corresponding acceptance of the spectrometers, as shown in the top panels of Figure 1. The spectra shown as full lines are from p+p collisions. In the bottom panels we plot nuclear modification factor  $R_{AA}$  and  $R_{CP}$  as a function of  $p_T$  for the most central collisions(0-10%) at  $\eta = 0, 1.0, 2.5, 3.0$  and  $3.5$ . The high  $p_T$  suppression persists over a wide range in pseudorapidity for the most central Au+Au collisions. For all pseudorapidities, the  $R_{AA}$  reaches a maximum value 0.6-0.7 at  $p_T \sim 2$  GeV/c, and then decreases. The  $R_{CP}$  shows the similar behavior. The observed behavior of nuclear modification factors seems to be consistent with jet surface emission picture [14]. Nuclear modification factors for identified charged hadrons,  $\pi^\pm$ ,  $K^\pm$ ,  $p$ , and  $\bar{p}$ , in 0-10% central Au+Au collisions at  $\sqrt{s_{NN}} = 200$  GeV are presented

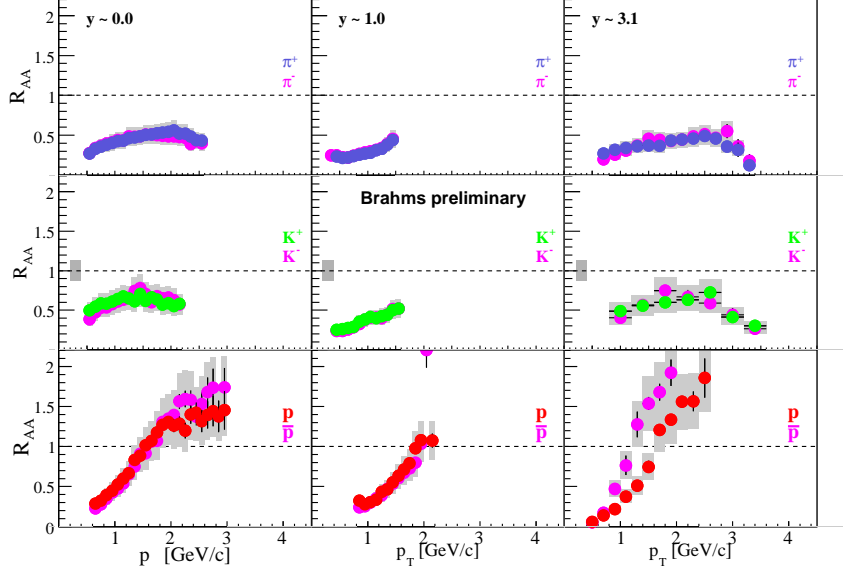


Figure 2. Nuclear modification factor  $R_{AA}$  for  $\pi^\pm$  (top),  $K^\pm$  (middle),  $p$ , and  $\bar{p}$  (bottom) at different rapidity for 0-10% centrality bins. Systematic errors are shown by the shaded boxes. The dotted lines indicate the expectation of binary scaling.

in Figure 2.  $R_{AA}$  for both positive and negative mesons exhibit the suppression at all measured rapidities, and shows very similar behavior at  $y \sim 0$  and  $y \sim 3.1$ . The protons and antiprotons show an enhancement in the intermediate  $p_T$  ranges, and we also see no significant change between the mid and forward rapidities for baryons. These observation might be related to the picture of the in-medium parton recombination process, which favors production of baryons over mesons at intermediate  $p_T$  region [15,16].

In order to get a better understanding on these mechanisms similar analysis has been done on the data in Au+Au and Cu+Cu collisions at  $\sqrt{s_{NN}} = 62.4$  GeV. The large suppression seen for Au+Au collisions at  $\sqrt{s_{NN}} = 200$  GeV is not observed at  $\sqrt{s_{NN}} = 62.4$  GeV. The nuclear modification factors for low energy and different systems are shown in Figure 3 and Figure 4. There is no significant difference between the measurements at midrapidity and at forward rapidity, however, the  $R_{AA}$  for 0-10% Cu+Cu collisions shows more enhancement than that of 0-10% Au+Au collisions. We see enhancement from central to more peripheral collisions, indicating geometry dependence of the system for nuclear modification factors.

The azimuthal anisotropy of emitted particles from heavy ion collisions is thought to be sensitive to the evolution of created matter, and believed to reflect to the information in early stage of collisions. The identified particle  $v_2(p_T)$  at midrapidity shows a strong dependence on  $p_T$ , and hydrodynamic calculations are in good agreement with the measurement up to about  $p_T \sim 1.5$  GeV/c [21,22]. The  $p_T$  differential elliptic flow of unidentified charged hadrons has also been measured at forward rapidities, showing a large dependence on  $p_T$  [23]. Figure 5 shows the elliptic flow  $v_2$  for identified charged particles as a function of  $p_T$  for 10-50% centrality bins at three different pseudorapidities by

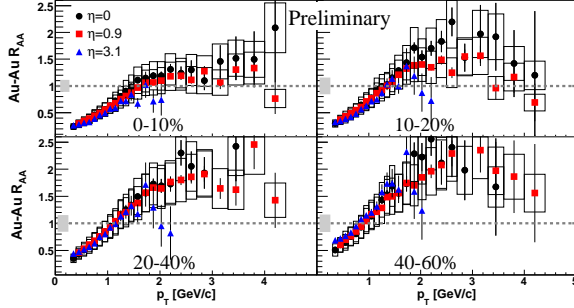


Figure 3.  $R_{AA}$  for Au+Au collisions at energy  $\sqrt{s_{NN}} = 62.4$  GeV. The midrapidity results,  $\eta = 0$  and  $0.9$  see [17]. The results at  $\eta = 3.1$  use BRAHMS own preliminary p+p reference data taken in the exact same pseudorapidity bin. The shaded bar at 1 shows the error on the scale.

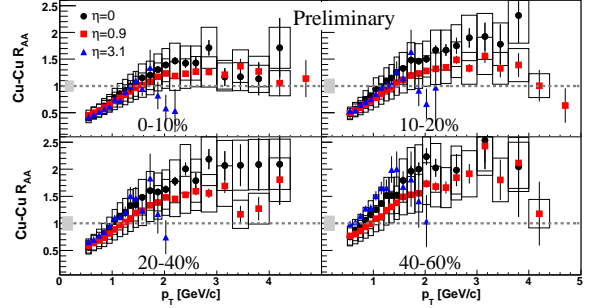


Figure 4.  $R_{AA}$  for Cu+Cu collisions at energy  $\sqrt{s_{NN}} = 62.4$  GeV. The midrapidity results,  $\eta = 0$  and  $0.9$ , use p+p reference spectra from ISR [18]. Systematic error for these results  $\sim 5\%$  on the scale. The shaded bar at 1 shows the error on the scale.

BRAHMS. The behavior for  $\pi^\pm$ ,  $K^\pm$ ,  $p$  and  $\bar{p}$  shows very little change with pseudorapidities. Hydrodynamic calculations with dissipative effects of the late hadronic expansion stage [19] reproduced data reasonably.

At a much later stage of collisions, light nuclei such as deuterons and antideuterons can be formed in the space-time evolution of a rapidly expanding system of nucleons [24]. Therefore, invariant yield of deuterons, compared to the protons from which they coalesce, provides information about the size of emitting system and space-time evolution. This ratio is defined as coalescence parameter  $B_2$ . The results of  $B_2$  as a function of  $p_T$  from Au+Au collisions at  $\sqrt{s_{NN}} = 200$  GeV are shown in Figure 6.  $B_2$  around midrapidity,  $y = 0$  and  $y \sim 1$ , shows increase for both particles and anti-particles, and this is consistent with an expanding source picture. But we cannot make any conclusions at forward rapidity with given results. Figure 7 shows the rapidity dependence of  $B_2$  for central Au+Au collisions at  $\sqrt{s_{NN}} = 200$  GeV. We see there is no significant dependence from  $y = 0$  to  $y = 3$ . The absence of a rapidity dependence for  $B_2$  might indicate that source volume does not change significantly in longitudinal direction.

### 3. Summary

In summary, BRAHMS measured charged hadron spectra over a broad range of rapidity and transverse momentum at both  $\sqrt{s_{NN}} = 62.4$  and  $\sqrt{s_{NN}} = 200$  GeV for several centrality bins. The nuclear modification factors  $R_{AA}$  and  $R_{CP}$  show very little variation with rapidity for both low and high energy. We find a suppression of  $R_{AuAu}$  at  $\sqrt{s_{NN}} = 200$  GeV extends to the forward rapidity,  $y = 3.5$ , for charged particles and identified particles. This indicates that hot and dense partonic matter is extended to the longitudinal direction. The little suppression of high  $p_T$  at  $\sqrt{s_{NN}} = 62.4$  GeV for Au+Au and Cu+Cu collisions shows the dependence of volume on colliding system. For the elliptic

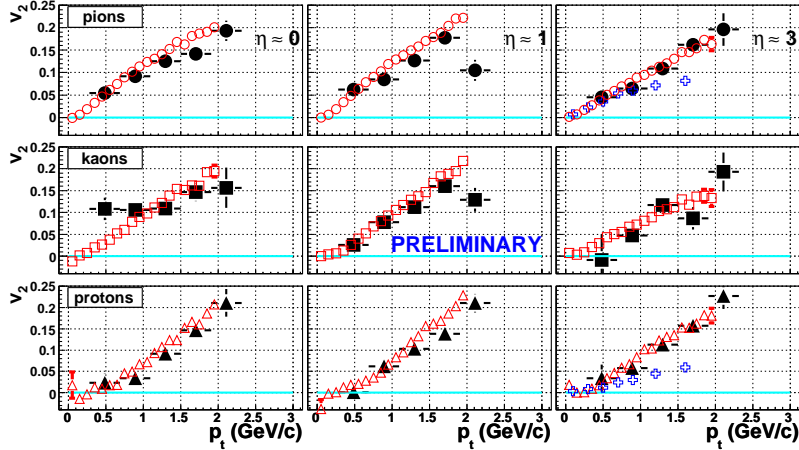


Figure 5.  $v_2(p_T, \eta)$  for pions, kaons, and protons (filled symbols). Theoretical values based on the hydrodynamic calculations of Hirano *et al.* [19] are shown by the open circles, squares, and triangles. The open crosses correspond to  $\eta \sim 4$  calculations using the AMPT model [20].

flow, we see that the pressure gradients remain constant in a longitudinally extended region. There is also no significant rapidity dependence of coalescence parameter, which means that the extent of the interaction region of freeze-out is almost constant over the measured rapidity range.

#### 4. Acknowledgments

This work was supported by the division of Nuclear Physics of the Office of Science of the U.S. DOE, the Danish Natural Science Research Council, the Research Council of Norway, the Polish State Committee for Scientific Research, the Romanian Ministry of Education and Research and Chonbuk National University(NP-2006-11).

#### REFERENCES

1. E. V. Shuryak, Phys. Lett. **B78**, 150 (1978).
2. J. C. Collins and P. J. Perry, Phys. Rev. Lett. **34**, 1353 (1975).
3. M. Adamczyk *et al*, BRAHMS Collaboration, Nucl. Instr. and Meth. **A499**, 437 (2003).
4. I. Arsene *et al*, BRAHMS Collaboration, Nucl. Phys. **A757**, 1-27 (2005).
5. Y. K. Lee, R. Debbé, J. H. Lee, H. Ito and S. Sanders, Nucl. Phys. **A516**, 281 (2004).
6. PHENIX Collaboration, Phys. Rev. Lett. **88**, 022301 (2002).
7. STAR Collaboration, Phys. Rev. Lett. **89**, 202301 (2002).
8. PHOBOS Collaboration, Phys. Lett. **B578**, 297 (2004).
9. BRAHMS Collaboration, Phys. Rev. Lett. **91**, 072305 (2003).
10. PHENIX Collaboration, Phys. Rev. Lett. **91**, 072303 (2002).

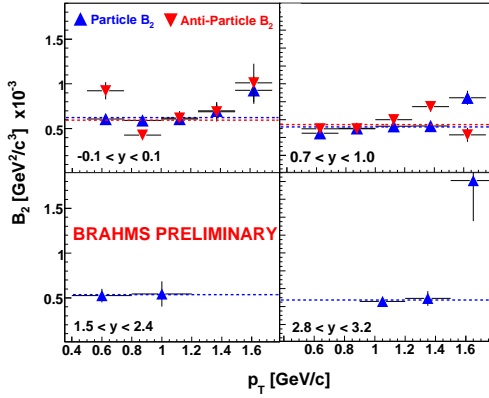


Figure 6. Particle and anti-particle  $B_2$  as a function of  $p_T$  at four rapidity intervals. The dashed horizontal lines are the weighted averages of each set of points.

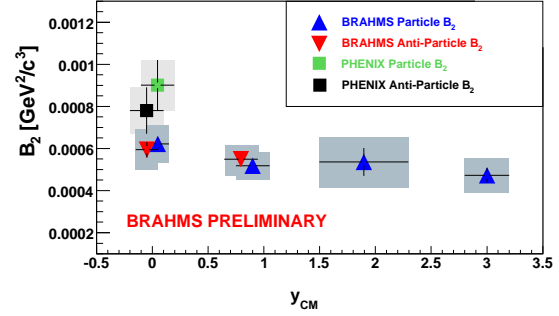


Figure 7. The coalescence parameter,  $B_2$  as a function of rapidity. The error bars and shaded error regions for the BRAHMS results indicate statistical and total uncertainties, respectively. Only total uncertainties are indicated for the PHENIX points [25].

11. STAR Collaboration, Phys. Rev. Lett. **91**, 072304 (2002).
12. PHOBOS Collaboration, Phys. Rev. Lett. **91**, 072302 (2002).
13. BRAHMS Collaboration, Phys. Rev. Lett. **93**, 242303 (2004).
14. K. J. Eskola, H. Honkanen, C. A. Salgado and U. A. Wiedemann, Nucl. Phys. **A747**, 511 (2005).
15. V. Greco, C. M. Ko, and I. Vitev *et al*, Phys. Rev. **C71**, 041901(R) (2005).
16. R. Hwa and C. B. Yang, Phys. Rev. **C70**, 024905 (2004).
17. I. Arsene *et al*, BRAHMS Collaboration, Submitted to Phys. Lett. B, nucl-ex/0602018.
18. D. d'Enterria, J. Phys. **G31** (2005) S491; Eur. Phys. J. **C43**, 295 (2005).
19. T. Hirano, U. W. Heinz, D. Kharzeev, R. Lacey and Y. Nara, Phys. Lett. **B636**, 299 (2006).
20. L. W. Chen, V. Greco, C. M. Ko and P. F. Kolb, Phys. Lett. **B605** 95 (2005).
21. J. Adams *et al.*, STAR Collaboration, Phys. Rev. Lett. **92**, 052302 (2004).
22. S. S. Adler *et al.*, PHENIX Collaboration, Phys. Rev. Lett. **91**, 182301 (2003).
23. J. Adams *et al.*, STAR Collaboration, Phys. Rev. **C72**, 014904 (2005).
24. A. Z. Mekjian, Phys. Rev. **C17**, 1051 (1978).
25. S. S. Adler *et al.*, PHENIX Collaboration, Phys. Rev. Lett. **94**, 122302 (2005).